

MIT Open Access Articles

Nonlinear XUV-optical transient grating spectroscopy at the Si L_{2,3}-edge

The MIT Faculty has made this article openly available. *Please share* how this access benefits you. Your story matters.

Citation: Bohinc, R. et al. "Nonlinear XUV-optical transient grating spectroscopy at the Si L_{2,3}-edge." Applied Physics Letters 114 (May 2019): 181101 © 2019 Author(s).

As Published: 10.1063/1.5085413

Publisher: AIP Publishing

Persistent URL: <https://hdl.handle.net/1721.1/130312>

Version: Final published version: final published article, as it appeared in a journal, conference proceedings, or other formally published context

Terms of Use: Article is made available in accordance with the publisher's policy and may be subject to US copyright law. Please refer to the publisher's site for terms of use.



Nonlinear XUV-optical transient grating spectroscopy at the Si $L_{2,3}$ -edge

Cite as: Appl. Phys. Lett. **114**, 181101 (2019); doi: [10.1063/1.5085413](https://doi.org/10.1063/1.5085413)

Submitted: 12 December 2018 · Accepted: 31 March 2019 ·

Published Online: 6 May 2019











View Online



Export Citation



CrossMark

R. Bohinc,^{1,a)}  G. Pamfilidis,¹ J. Rehault,¹ P. Radi,¹  C. Milne,¹  J. Szlachetko,² F. Bencivenga,³  F. Capotondi,³ R. Cucini,⁴ L. Foglia,³  C. Masciovecchio,³ R. Mincigrucci,³ E. Pedersoli,³  A. Simoncig,³ N. Mahne,⁵  A. Cannizzo,⁶ H. M. Frey,⁶ Z. Ollmann,⁶ T. Feurer,⁶ A. A. Maznev,⁷ K. Nelson,⁷ and G. Knopp¹ 

AFFILIATIONS

¹Paul Scherrer Institut (PSI), 5232 Villigen PSI, Switzerland

²Institute of Nuclear Physics, Polish Academy of Sciences, 31-342 Kraków, Poland

³Elettra-Sincrotrone Trieste S.C.p.A., S.S. 14 km 163,5 in Area Science Park, I-34012 Basovizza, Trieste, Italy

⁴Istituto Officina dei Materiali-CNR, 34149 Basovizza (TS), Italy

⁵IOM-CNR, Strada Statale 14 km 163.5, 34149 Basovizza, Trieste, Italy

⁶Institute of Applied Physics, University of Bern, 3012 Bern, Switzerland

⁷Massachusetts Institute of Technology, Cambridge, Massachusetts 02139, USA

^{a)} Author to whom correspondence should be addressed: rok.bohinc@psi.ch

ABSTRACT

Time-resolved transient grating (TG) spectroscopy facilitates detailed studies of electron dynamics and transport phenomena by means of a periodic excitation of matter with coherent ultrashort light pulses. Several current and next generation free-electron laser (FEL) facilities provide fully coherent pulses with few femtosecond pulse durations and extreme ultraviolet (XUV) photon energies. Thus, they allow for transient grating experiments with periodicities as small as tens of nanometers and with element specific photon energies. Here, we demonstrate the element specificity of XUV TG (X-TG) experiments by tuning the photon energy across the Si $L_{2,3}$ -edge of Si_3N_4 . We observe a shortening of the signal decay when increasing the XUV photon energy above the absorption edge. The analysis of the wavelength dependent signal shows that the faster decay is driven by the increase in the charge carrier density. From the decay constants the interband Auger coefficient at elevated temperatures and high electron densities has been determined.

Published under license by AIP Publishing. <https://doi.org/10.1063/1.5085413>

Nonlinear interaction of light with matter provides a powerful tool to study dynamical processes in microscopic systems. Although the majority of advances in nonlinear spectroscopy over the last few decades were made in the optical regime, the feasibility to observe nonlinear processes in materials is in principle not bound by the frequency of interacting fields. While the excitation of matter with optical and UV light promotes electronic transitions from the valence band, the frequency of XUV light and X-rays is sufficient to excite core-shell electrons. X-ray scattering typically shows a resonant behavior when the photon energy is tuned near an atomic absorption edge of an element. Unlike optical photons, X-rays selectively probe the electronic structure of elements, conferring high locality to X-ray spectroscopic methods. X-ray induced core-valence transitions provide insight into electron correlations and can therefore provide information about coupling mechanisms, coherence, and dynamics with an almost atomic resolution and specification.¹

To date, nonlinear X-ray processes, such as parametric down-conversion,² X-ray second-harmonic generation,^{3,4} X-ray/optical sum-frequency generation,⁵ stimulated emission/Raman,⁶ nonlinear Compton scattering,⁷ two-photon absorption^{8,9} and emission,⁸ and two-photon ionization^{10,11} have been realized. These rather static approaches rely on detecting characteristic (e.g., spectrally resolved) photon or electron emissions at increased X-ray intensities. Charge carrier dynamics at ultrafast timescales down to the attosecond regime have been performed by optical pump XUV-probe experiments using lab based HHG sources.¹²⁻¹⁴ X-ray nonlinear methodologies that comprise temporal information are scarce. With the development of X-ray FEL sources to produce fully coherent fs X-ray pulses, however, time-resolved X-ray four wave mixing (X-FWM) experiments became potentially feasible. Due to spatial and temporal signal dependences, X-FWM has the capability to measure quantum state correlations, coherent motions, and electron dynamics. Up to now, FEL based

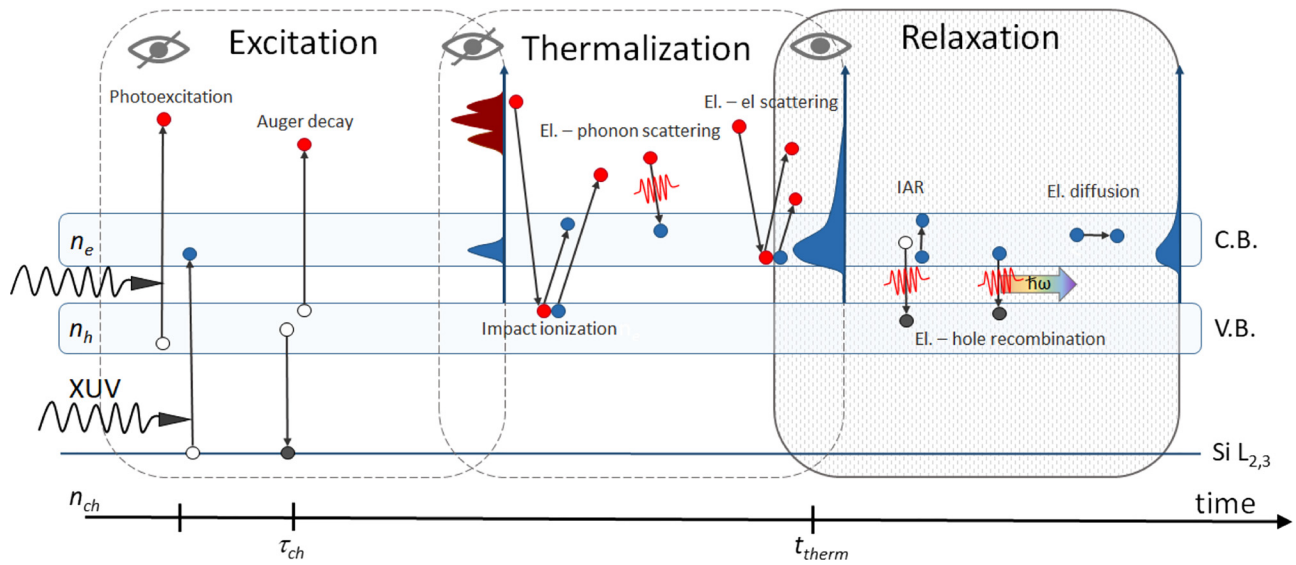


FIG. 1. Schematic representation of the charge carrier dynamics after the excitation of Si_3N_4 at the $\text{Si L}_{2,3}$ edge. “Hot” and “cold” electrons are shown in red and blue, respectively, and phonons are depicted as red oscillatory lines. Although excitation, thermalization, and relaxation are depicted as three different phases, they occur simultaneously, which is indicated by overlapping dashed and full lines.

X-FWM has been demonstrated in a transient grating (TG) configuration for excitation energies in the XUV regime far below typical core-ionization thresholds.^{15–17} In this work, we report time and energy-dependent X-TG measurements on Si_3N_4 membranes with excitation energies tuned around the $\text{Si L}_{2,3}$ -edge.

In the X-TG configuration, an interference pattern from two crossed coherent FEL pulses with frequency ω_{FEL} is produced at the sample position initiating the dynamics of charge carriers and nuclei (see Fig. 1). The periodicity of the induced grating can be matched to system relevant distances and allows the investigation on micro- (atom, molecule, lattice, and quantum mechanics), meso- (correlated spin, electron, complex matter, and many particle systems),¹⁸ and macroscopic length scales (transport phenomena).¹⁹ The absorption of X-ray photons creates electron-hole pairs in the position of the fringes. If the X-ray energy is tuned above the core-ionization thresholds, the created core-holes are subsequently filled with electrons from higher energy levels. For low Z materials, the core-hole decay occurring on the fs time scale, e.g., $\tau_{\text{ch}} \sim 10$ fs for $\text{Si L}_{2,3}$ -edge,²⁰ is accompanied by the release of a hot Auger electron. The thermalization of hot electrons is mediated through electron-electron scattering, with the associated thermalization time highly dependent on electron energy and charge carrier density,²¹ and electron-phonon scattering responsible for the generation of acoustic and optical phonons. While for optical and UV-excitations, thermalization time t_{therm} is considered to be in the range of tens to hundreds of fs depending on the material and excitation conditions,^{12,22,23} thermalization of electrons with kinetic energies much higher than the bandgap energy is even faster (<25 fs) due to impact ionization.^{24,25} The augmentation of the charge carrier density through impact ionization can amount to an order of magnitude of the initial charge carrier density in the XUV range, depending on the density of states and the ratio between the excitation energy and the bandgap energy.

After thermalization, electrons and holes are in a near-equilibrium state with the same spatial distribution as ensured by the

Dember effect. Assuming a negligible proportion of electrons escaping the material, electrons and holes contribute equally to the charge carrier density n . The charge carrier dynamics after thermalization is driven by impact ionization, electron hole recombination, interband Auger recombination (IAR), and charge carrier diffusion.^{26,27} At high charge carrier densities, IAR processes become the dominant decay mechanism on the short time scale^{28–30} and can be described as²⁶

$$\frac{\partial n(t > t_{\text{therm}}, x)}{\partial t} = -\gamma_{\text{au}} n^3(t, x), \quad (1a)$$

$$n(t = t_{\text{therm}}, x) = n_0 \frac{1 - \cos\left(\frac{2\pi x}{\Lambda}\right)}{2}, \quad (1b)$$

where γ_{au} and Λ are the IAR constant and the periodicity of the induced grating, respectively. The three particle recombination process, involving two conduction band electrons and a hole in the valence band, can be mediated by electron-phonon scattering. The charge carrier density modulation is considered to depend only on the x -direction across the induced grating. Equation (1b) specifies the initial condition, with n_0 being the maximal charge carrier density in the center of the fringes after thermalization. An analytical solution to Eq. (1a) is given by

$$n_{\text{Au}}(t, x) = n_0 \frac{1 - \cos\left(\frac{2\pi x}{\Lambda}\right)}{2} \frac{1}{\sqrt{1 + 8 \frac{t}{\tau_{\text{Au}}}}}, \quad \tau_{\text{Au}} = \frac{4}{n_0^2 \gamma_{\text{Au}}}, \quad (2)$$

where τ_{Au} is referred to as the Auger lifetime. It is important to note that the Auger lifetime strongly depends on the initial charge carrier density n_0 .

The time-evolution of the charge carrier density is directly reflected in the changes of the refractive index. It is therefore possible

to follow charge carrier dynamics induced by the two XUV-FEL pulses by probing the induced excitation with a third, time-delayed optical/UV pulse. The measured X-TG signal $I_{TG}(\delta t, \vec{r})$ is proportional to the absolute squared third order polarization $P_{TG}^{(3)}$ and depends on the evolution of the charge carrier density

$$I_{TG}(\delta t, \vec{r}) \propto \int_{-\infty}^{\infty} |P_{TG}^{(3)}(t, \delta t, \vec{r})|^2 dt, \quad (3)$$

where δt is the delay between the XUV pump pulses and the optical probe pulse. Signals are observed in a phase matched direction $\vec{k}_s = \vec{q} + \vec{k}_{pr}$, where \vec{k}_{pr} is the probe pulse wavevector and $|\vec{q}| = \frac{2\pi}{\Lambda}$. Without specific probe pulse resonances and far from saturation, the TG intensity simplifies to

$$I_{TG}(\delta t, x) \propto n^2(\delta t, x) I_{pr} L^2 \text{sinc}^2\left(\frac{\Delta k L}{2}\right), \quad (4)$$

where Δk is the wavevector mismatch and L is the coherence length of interaction well approximated with the XUV absorption length.

The X-TG FWM experiments were performed at the DIPROI endstation of the FERMI FEL. The FERMI FEL 2 laser source, seeded by an OPA output, was used to generate XUV laser pulses with a duration of about 40 fs FWHM at a repetition frequency of 50 Hz.³¹ The initial photon energy was set to 101.3 eV (harmonics M7 N3 of the FEL II laser system). Tunability of the FEL 2 output was achieved by tuning the seed laser wavelength between 245 nm and 265 nm or by switching the harmonic combination of the two radiator sections of FEL 2 to cover a range of 86 eV to 115 eV with a bandwidth of about 40 meV. The average XUV pulse power during scans was varying between 2 and 4 $\mu\text{J}/\text{pulse}$. By manipulating the incoming FEL pulses with the MINI-TIMER split and delay setup, an interference pattern of size $140 \times 140 \mu\text{m}^2$ FWHM was created on a 200 nm thick amorphous Si_3N_4 membrane. Si_3N_4 membranes are routinely used as timing tools at FEL facilities because of their strong reflectivity change when impinging with X-rays. The FEL induced changes in the refractive index were probed by an optical (397.5 nm) probe-pulse with a duration of about 100 fs FWHM. Similar to the pump beams, the probe beam was vertically polarized. A FEL crossing angle of about $2\theta = 2.6^\circ$ was adapted to achieve comparable fringe spacing ($\Lambda \sim 270$ nm). Due to an angle of $\alpha = 45^\circ$ of the probe-pulse with respect to the surface normal, the effective pulse duration increased to yield an estimated total experimental resolution of (210 ± 33) fs. The TG-signals were detected on an in-vacuum 2048×2048 square pixel CCD detector with a pixel size of $13.5 \mu\text{m}$, positioned at $\beta = -45^\circ$ from the normal of the surface behind the sample. Figure 2 shows a scheme of the experimental setup, described in detail previously,¹⁵ and typical signals observed during the measurements. The measurements at a specific time-delay were performed by integrating the signal over the region of interest on the CCD over 100 to 500 shots, depending on the signal strength. X-TG signals were detected for time delays between -3 and 120 ps on a logarithmic scale to allow us to cover a large dynamic range with an adequate resolution. The data acquisition time for a scan was around 1 to 2 h, and no formation of permanent grating due to sample damage has been observed within this time. Data treatment is discussed in the [supplementary material](#). The XUV absorption spectra of amorphous Si_3N_4 membranes have been measured in the transmission mode at the BEAR beamline of the Elettra Synchrotron.

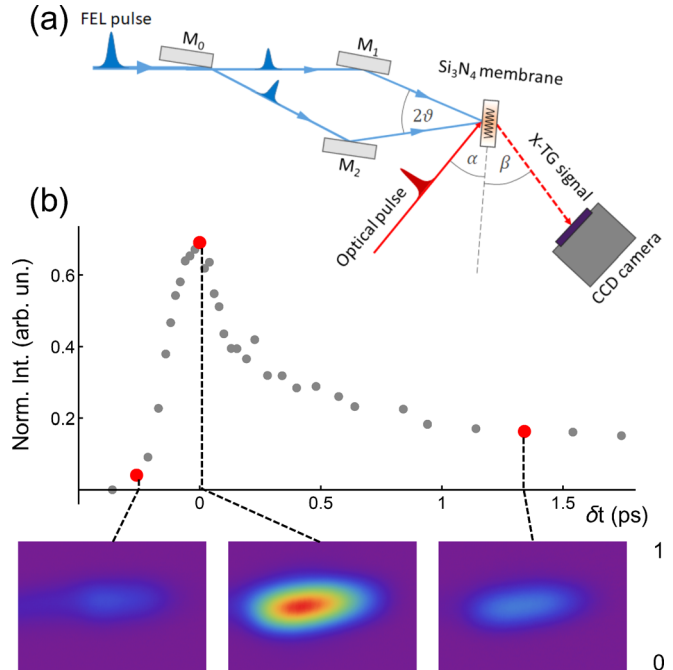


FIG. 2. (a) Scheme of the MINI-TIMER setup for performing FWM experiments. The incident XUV pulse (blue) is split (mirror M_0) and combined (mirrors M_1 and M_2) at the sample position to be mixed with a temporally delayed optical pulse (red). The transmitted X-TG signal is detected using a CCD detector. (b) X-TG signals as observed on the CCD detector and the corresponding time trace for 100 eV XUV excitation. The time delays δt for which the CCD images are shown are marked red in the time trace.

The monochromator slits were set at $50 \mu\text{m}$ to yield an energy resolution of about 10^{-2} eV at 100 eV.

A series of X-TG time traces corresponding to excitation energies ranging from 86 eV to 115 eV has been recorded for amorphous Si_3N_4 membranes. Figure 3 compares time traces recorded for excitation energies above and below the Si $L_{2,3}$ absorption edge. The two signals show similar characteristics: A fast rise, a decay on a short sub-ps time scale, and an almost persistent contribution for long delay times. The latter dynamics originating from thermal diffusion will be discussed elsewhere and is not further considered in the analysis of our data. Time traces corresponding to excitations above and below the absorption edge mainly differ on short time scales. In particular, the above-edge time trace shows a faster decay compared to the below-edge time trace, indicating a higher initial charge density [see Eq. (2)]. An excitation below the absorption edge yields hot photoelectrons originating from valence [Si(3p) and N(2p) orbitals] and inner-valence [Si(3p, 3s) and N(2s) orbitals] bands. The increase in the photon energy above the absorption edge, on the other hand, additionally permits electrons from the core level and the corresponding Auger electrons to be excited into the conduction band causing a decrease in the XUV attenuation length from 193 nm to 54 nm.

To extract quantitative information from our data, transient signals were fitted by a global fitting algorithm in which thermalization was neglected. The temporal characteristics of the observed TG-signals could be well reproduced within our model (see [supplementary](#)

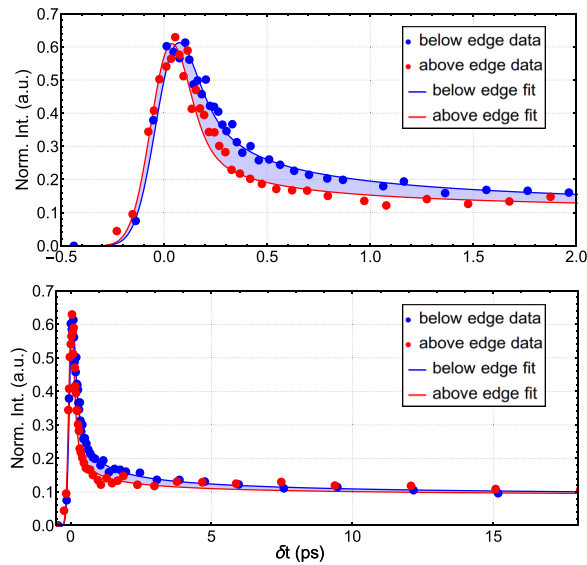


FIG. 3. Transient signals corresponding to excitation energies below (101 eV) and above (104.5 eV) the absorption edge. The upper graph is an enlarged image of the lower graph at short time delays.

material). The fit indicates an experimental resolution of 207 fs, which is close to the predicted experimental resolution, justifying the application of the instantaneous thermalization model. The obtained Auger lifetimes, shown in Fig. 4, indicate a steep drop from (99 ± 14) fs to (0.6 ± 0.5) fs located around 103 eV. The extracted values correspond to the decay time in the charge carrier density and are not to be confused with the decay of the transient signal. The obtained Auger lifetimes are compared with the Si $L_{2,3}$ XUV-absorption spectrum of amorphous Si_3N_4 . The spectrum exhibits a broad white line positioned at 105 eV with a long tail toward lower energies attributed to the presence of defects. The step in the Auger lifetime shown in Fig. 4 coincides with the Si $L_{2,3}$ absorption edge of amorphous Si_3N_4 , in agreement with the interpretation of our data in terms of an energy dependent initial charge carrier density. Expanding our model with respect to thermalization, a constant increase in the extracted Auger lifetimes is obtained. The position and magnitude of the step in the Auger lifetime are, however, not influenced by the inclusion of a finite thermalization time (see supplementary material). For a correct interpretation of our data, care has to be taken because an increase in the FEL intensity can modify the signal decay in a similar way as the opening of the core-excitation channel. In the data presented, the FEL intensity I_{XUV} , given in the lower part of Fig. 4, slightly decreases with photon energy ω_{XUV} , and therefore, no correlation between the faster decay at energies above the absorption edge and the applied intensities is found. Our results therefore demonstrate that FEL based XUV TG-FWM experiments are capable of measuring electron dynamics as a function of the X-ray absorption process.

The dependence of the Auger lifetimes on the initial charge carrier density, deduced from measurements of the XUV attenuation length, exhibits a near quadratic dependence as predicted by Eq. (2) (see Fig. S10). From the extracted Auger lifetimes and the initial charge carrier densities, we estimate an IAR coefficient of $(1.2 \pm 1.3) \times 10^{-29}$

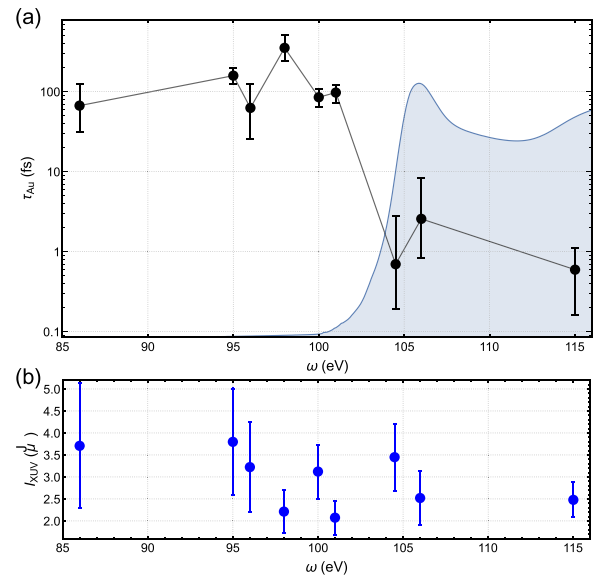


FIG. 4. (a) Fitted values of Auger lifetimes (black) along with the Si $L_{2,3}$ XUV-absorption spectrum of amorphous Si_3N_4 (blue). (b) XUV intensities during the corresponding measurements.

$\text{cm}^6 \text{s}^{-1}$ in the instantaneous thermalization model (see supplementary material). Applying the Auger lifetimes extracted in the model of maximal thermalization, a lower limit for the IAR coefficient of $(3.1 \pm 3.6) \times 10^{-31} \text{ cm}^6 \text{ s}^{-1}$ is deduced. The accuracy of these limiting values is compromised by an approximate estimation of the multiplication factor, i.e., the amount of charge carriers created through impact ionization by a hot electron.²⁴ For the possible contribution of electron diffusion to the X-TG signal, we estimate a relative systematic error in the obtained IAR coefficient of 37% (see supplementary material). The estimated limits of the IAR coefficient agree with the IAR coefficients of other materials ranging from $10^{-25} \text{ cm}^6 \text{ s}^{-1}$ to $10^{-32} \text{ cm}^6 \text{ s}^{-1}$.^{32–35} The coefficient increases with increasing temperature and density and decreasing bandgap related activation energy.³⁴ As Si_3N_4 has an indirect bandgap of about 5.5 eV, the associated Auger coefficient is expected to be small at room temperature. However, the conditions in our experiment yielded a lattice temperature close to the melting temperature of the material at 2170 K and high charge carrier densities increasing the value of the IAR coefficient.

A more accurate estimation of the IAR coefficient than the one presented in this work is possible for measurements in which the charge carrier density can precisely be determined. In the photo-induced luminescence from band to band recombination of highly doped semiconductors, the dependence of the minority carrier Auger lifetime on the majority carrier density is measured.^{32,33} The concentration of majority carrier density can accurately be determined by measuring the resistivity and the Hall coefficient of the material. The IAR coefficient can also be determined by measuring reflectivity and transmission changes induced by laser light at frequencies near the bandgap.^{35,36} For such excitations, the charge carrier density can easily be determined from laser power measurements as thermalization of excited electrons does not augment the charge carrier density. In both methods, the Auger lifetime is determined for time delays much longer than thermalization time, enabling a

precise determination of the IAR coefficient. Measurements at long time delays, however, restrict the determination of the IAR coefficient for charge carrier density lower than $\sim 10^{20} \text{ cm}^{-3}$. FEL based X-TG measurements, on the other hand, provide access to IAR coefficients for significantly higher charge carrier densities.

In this work, we have demonstrated time and energy resolved X-TG experiments on Si_3N_4 membranes with the excitation energy tuned around the Si $L_{2,3}$ absorption edge. The induced charge carrier dynamics indicated a fast signal decay due to IAR. The increase in the incident XUV energy above the Si $L_{2,3}$ edge resulted in higher initial charge carrier densities and consequently faster decay times of the observed TG signal. A fitting analysis of the measured time traces indicated a sharp decrease in the Auger lifetime at the position of the absorption edge. The possibility to combine the X-FWM approach with the atomic selectivity provided by XUV/X-ray photons may open up the way for a manifold of studies on ultrafast processes and correlations with chemical sensitivity.

See [supplementary material](#) for information about the X-TG light-matter interaction, charge carrier dynamics, signal modeling, UV-Vis spectra, data treatment, and IAR coefficient.

The research leading to these results has received funding from the Swiss National Science Foundation (SNF) under Grant Agreement No. 200021_165550/1. J.S. acknowledges partial support from the National Science Center Poland (NCN) under Grant No. 2015/19/B/ST2/00931. A.C., H.M.F., Z.O., and T.F. acknowledge funding by the NCCR MUST research instrument of the Swiss National Science Foundation.

REFERENCES

- S. Mukamel, D. Healion, Y. Zhang, and J. D. Biggs, *Annu. Rev. Phys. Chem.* **64**, 101 (2013).
- S. Schwartz, R. N. Coffee, J. M. Feldkamp, Y. Feng, J. B. Hastings, G. Y. Yin, and S. E. Harris, *Phys. Rev. Lett.* **109**, 013602 (2012).
- S. Schwartz, M. Fuchs, J. B. Hastings, Y. Inubushi, T. Ishikawa, T. Katayama, D. A. Reis, T. Sato, K. Tono, M. Yabashi, S. Yudovich, and S. E. Harris, *Phys. Rev. Lett.* **112**, 163901 (2014).
- R. K. Lam, S. L. Raj, T. A. Pascal, C. D. Pemmaraju, L. Foglia, A. Simoncig, N. Fabris, P. Miotti, C. J. Hull, A. M. Rizzuto, J. W. Smith, R. Mincigrucchi, C. Masciovecchio, A. Gessini, E. Allaria, G. De Ninno, B. Diviacco, E. Roussel, S. Spampinati, G. Penco, S. Di Mitri, M. Trovò, M. Danailov, S. T. Christensen, D. Sokaras, T.-C. Weng, M. Coreno, L. Poletto, W. S. Drisdell, D. Prendergast, L. Giannessi, E. Principi, D. Nordlund, R. J. Saykally, and C. P. Schwartz, *Phys. Rev. Lett.* **120**, 023901 (2018).
- T. E. Glover, D. M. Fritz, M. Cammarata, T. K. Allison, S. Coh, J. M. Feldkamp, H. Lemke, D. Zhu, Y. Feng, R. N. Coffee, M. Fuchs, S. Ghimire, J. Chen, S. Schwartz, D. A. Reis, S. E. Harris, and J. B. Hastings, *Nature* **488**, 603 (2012).
- M. Beye, S. Schreck, F. Sorgenfrei, C. Trabant, N. Pontius, C. Schüßler-Langeheine, W. Wurth, and A. Föhlisch, *Nature* **501**, 191 (2013).
- M. Fuchs, M. Trigo, J. Chen, S. Ghimire, S. Schwartz, M. Kozina, M. Jiang, T. Henighan, C. Bray, G. Ndabashimiye, P. H. Bucksbaum, Y. Feng, S. Herrmann, G. A. Carini, J. Pines, P. Hart, C. Kenney, S. Guillet, S. Boutet, G. J. Williams, M. Messerschmidt, M. M. Seibert, S. Moeller, J. B. Hastings, and D. A. Reis, *Nat. Phys.* **11**, 964–970 (2015).
- J. Szlachetko, J. Hoszowska, J.-C. Dousse, M. Nachttegaal, W. Bachucki, Y. Kayser, J. Sá, M. Messerschmidt, S. Boutet, G. J. Williams, C. David, G. Smolentsev, J. A. van Bokhoven, B. D. Patterson, T. J. Penfold, G. Knopp, M. Pajek, R. Abela, and C. J. Milne, *Sci. Rep.* **6**, 33292 (2016).
- K. Tamasaku, E. Shigemasa, Y. Inubushi, T. Katayama, K. Sawada, H. Yumoto, H. Ohashi, H. Mimura, M. Yabashi, K. Yamauchi, and T. Ishikawa, *Nat. Photonics* **8**, 313–316 (2014).
- T. Mazza, A. Karamatskou, M. Ilchen, S. Bakhtiarzadeh, A. J. Rafipoor, P. O’Keeffe, T. J. Kelly, N. Walsh, J. T. Costello, M. Meyer, and R. Santra, *Nat. Commun.* **6**, 6799 (2015).
- T. Sekikawa, A. Kosuge, T. Kanai, and S. Watanabe, *Nature* **432**, 605–608 (2004).
- S. K. Cushing, M. Zürich, P. M. Kraus, L. M. Carneiro, A. Lee, H.-T. Chang, C. J. Kaplan, and S. R. Leone, *Struct. Dyn.* **5**, 054302 (2018).
- M. Schultze, K. Ramasesha, C. Pemmaraju, S. Sato, D. Whitmore, A. Gandman, J. S. Prell, L. J. Borja, D. Prendergast, K. Yabana, D. M. Neumark, and S. R. Leone, *Science* **346**, 1348 (2014).
- M. Zürich, H.-T. Chang, P. M. Kraus, S. K. Cushing, L. J. Borja, A. Gandman, C. J. Kaplan, M. H. Oh, J. S. Prell, D. Prendergast, C. D. Pemmaraju, D. M. Neumark, and S. R. Leone, *Struct. Dyn.* **4**, 044029 (2017).
- F. Bencivenga, A. Calvi, F. Capotondi, R. Cucini, R. Mincigrucchi, A. Simoncig, M. Manfredda, E. Pedersoli, E. Principi, F. Dallari, R. A. Duncan, M. G. Izzo, G. Knopp, A. A. Maznev, G. Monaco, S. Di Mitri, A. Gessini, L. Giannessi, N. Mahne, I. P. Nikolov, R. Passuello, L. Raimondi, M. Zangrando, and C. Masciovecchio, *Faraday Discuss.* **194**, 283 (2016).
- F. Bencivenga, R. Cucini, F. Capotondi, A. Battistoni, R. Mincigrucchi, E. Giangrisostomi, A. Gessini, M. Manfredda, I. P. Nikolov, E. Pedersoli, E. Principi, C. Svetina, P. Parisse, F. Casolari, M. B. Danailov, M. Kiskinova, and C. Masciovecchio, *Nature* **520**, 205–208 (2015).
- L. Foglia, F. Capotondi, R. Mincigrucchi, D. Naumenko, E. Pedersoli, A. Simoncig, G. Kurdi, A. Calvi, M. Manfredda, L. Raimondi, N. Mahne, M. Zangrando, C. Masciovecchio, and F. Bencivenga, *Phys. Rev. Lett.* **120**, 263901 (2018).
- J. Janusonis, T. Jansma, C. L. Chang, Q. Liu, A. Gatilova, A. M. Lomonosov, V. Shalagatski, T. Pezeril, V. Temnov, and R. I. Tobey, *Nat. Sci. Rep.* **6**, 29143 (2016).
- A. A. Maznev, F. Bencivenga, A. Cannizzo, F. Capotondi, R. Cucini, R. A. Duncan, T. Feuerer, T. D. Frazer, L. Foglia, H.-M. Frey, H. Kapteyn, J. Knobloch, G. Knopp, C. Masciovecchio, R. Mincigrucchi, G. Monaco, M. Murnane, I. Nikolov, E. Pedersoli, A. Simoncig, A. Vega-Flick, and K. A. Nelson, *Appl. Phys. Lett.* **113**, 221905 (2018).
- J. Campbell and T. Papp, *At. Data Nucl. Data Tables* **77**, 1 (2001).
- A. Othonos, *J. Appl. Phys.* **83**, 1789 (1998).
- J. R. Goldman and J. A. Prybyla, *Phys. Rev. Lett.* **72**, 1364 (1994).
- E. Baldini, T. Palmieri, E. Pomarico, G. Auböck, and M. Chergui, *ACS Photonics* **5**, 1241 (2018).
- N. Medvedev and B. Rethfeld, *New J. Phys.* **12**, 073037 (2010).
- J. B. Sambur, T. Novet, and B. A. Parkinson, *Science* **330**, 63 (2010).
- A. Rämér, O. Osmani, and B. Rethfeld, *J. Appl. Phys.* **116**, 053508 (2014).
- H. M. van Driel, *Phys. Rev. B* **35**, 8166 (1987).
- S. Boubanga-Tombet, J. B. Wright, P. Lu, M. R. C. Williams, C. Li, G. T. Wang, and R. P. Prasankumar, *ACS Photonics* **3**, 2237 (2016).
- R. Vaxenburg, A. Rodina, A. Shabaev, E. Lifshitz, and A. L. Efros, *Nano Lett.* **15**, 2092 (2015).
- A. Haug, *J. Phys. C: Solid State Phys.* **16**, 4159 (1983).
- E. Allaria, D. Castronovo, P. Cinquegrana, P. Craievich, M. Dal Forno, M. B. Danailov, G. D’Auria, A. Demidovich, G. De Ninno, S. Di Mitri, B. Diviacco, W. M. Fawley, M. Ferianis, E. Ferrari, L. Froehlich, G. Gaio, D. Gauthier, L. Giannessi, R. Ivanov, B. Mahieu, N. Mahne, I. Nikolov, F. Parmigiani, G. Penco, L. Raimondi, C. Scafuri, C. Serpico, P. Sigalotti, S. Spampinati, C. Spezzani, M. Svandrik, C. Svetina, M. Trovo, M. Veronese, D. Zangrando, and M. Zangrando, *Nat. Photonics* **7**, 913 (2013).
- J. Dziewior and W. Schmid, *Appl. Phys. Lett.* **31**, 346 (1977).
- J. Beck and R. Conradt, *Solid State Commun.* **13**, 93 (1973).
- K. L. Kioupakis, D. Steiauf, P. Rinke, K. T. Delaney, and C. G. Van de Walle, *Phys. Rev. B* **92**, 035207 (2015).
- D. G. McLean, M. G. Roe, A. I. D’Souza, and P. E. Wigen, *Appl. Phys. Lett.* **48**, 992 (1986).
- K. L. Vodopyanov, H. Graener, C. C. Phillips, and T. J. Tate, *Phys. Rev. B* **46**, 13194 (1992).